

2014

Applying Automated Tracking of Microtubules by plusTipTracker

Cody Andrew Molnar
Lehigh University

Follow this and additional works at: <http://preserve.lehigh.edu/etd>

 Part of the [Molecular Biology Commons](#)

Recommended Citation

Molnar, Cody Andrew, "Applying Automated Tracking of Microtubules by plusTipTracker" (2014). *Theses and Dissertations*. Paper 1562.

This Thesis is brought to you for free and open access by Lehigh Preserve. It has been accepted for inclusion in Theses and Dissertations by an authorized administrator of Lehigh Preserve. For more information, please contact preserve@lehigh.edu.

Applying Automated Tracking of Microtubules by plusTipTracker

by

Cody A. Molnar

A Thesis

Presented to the Graduate and Research Committee

of Lehigh University

in Candidacy for the Degree of

Master of Sciences

in

Molecular Biology

Lehigh University

April 25, 2014

© 2014 Copyright
Cody A. Molnar

Thesis is accepted and approved in partial fulfillment of the requirements for the Master of Science in Molecular Biology.

Automated Tracking of Microtubules Using plusTipTracker
Cody A. Molnar

April 25, 2014

Lynne Cassimeris

Murray Itzkowitz

TABLE OF CONTENTS

List of Figures	(v)
List of Tables	(vi)
Abstract	1
Introduction	2
Microtubules and Dynamics	2
Stathmin, A Microtubule Regulator	3
Taxol, p53 and Microtubules	4
Figures	7
Results	
Establishing and Determining a Standard Procedure	8
Figures and Tables	10
Stathmin and p27	16
Figures and Tables	19
Taxol and p53	26
Figures and Tables	28
Discussion	36
Methods	39
References	41
Vita	45

LIST OF FIGURES

Figure 1: Microtubule Dynamics and Comet Structures

Figure 2: Mechanism of Stathmin Regulation of Microtubules in Cells

Figure 3: Comet detection

Figure 4: Parameter Determination of Comet Size

Figure 5: Parameter Determination of Backward and Forward Angles

Figure 6: Parameter Determination of Shrinkage Factor and Fluctuation Radius

Figure 7: Parameter Determination of Time Window

Figure 8: p27/Stathmin Influences Microtubule Dynamics

Figure 9: Experimental Conditions do not Affect Comets

Figure 10: Restoration of p53 in HeLa cells

LIST OF TABLES

Table 1: Dynamics of Control Cells

Table 2: Dynamics of Stamina-Depleted Cells

Table 3: Dynamics of p27-Depleted Cells

Table 4: Dynamics of co-depletion of p27/Stathmin

Table 5: Dynamics of 10 nM Taxol Treated Cells

Table 6: Dynamics of p53 Restored Cells

Table 7: Dynamics of p53 Restored and 10 nM Taxol Treated Cells

Table 8: p53 Restoration Alters Response to Taxol Treatment

ABSTRACT

Automated microtubule tracking programs have potential as a powerful tool for analyzing a variety of experimental conditions. Here, we apply one such program, plusTipTracker, developed by the Danuser lab, to investigate the effects of stathmin and p27 depletion on microtubule dynamics. We also apply plusTipTracker to analyze the relationship between p53 and taxol on microtubule dynamics. By developing a standardized procedure, we were able to streamline the detection and analysis of these conditions much faster than is possible by hand. We found that both p27 and stathmin depletion alter microtubule dynamics. This is proposed to be a result of p27 binding to stathmin and competing for stathmin's tubulin-sequestering abilities *in vivo*. p53 was found to repress microtubule dynamics in interphase HeLa cells. Taxol was also found to greatly repress microtubule dynamics, and this repression is augmented by the presence of p53. Based on these observations and results, we conclude plusTipTracker is a powerful method for the analysis of microtubules under our conditions.

Introduction

Cells possess a highly dynamic and flexible skeleton of microtubules (MT) composed of tubulin subunits that can self-polymerize. Microtubules are responsible for a variety of cellular processes, including chromosome separation, vesicle transport, polarization, localizing scaffolds and cell movement. To perform such a wide array of functions, microtubules are dynamic and can switch from growth to shrinking, and an event termed catastrophe, and from shrinkage to growth, an event termed rescue. Microtubules can also exhibit periods of very slow or nonexistent growth with no loss of total length. This is termed 'pausing' (Mitchison and Kirshner, 1984). A schematic for this behavior is shown in figure 1.1. Microtubules are also highly polarized, with most growth and activity occurring at the 'plus' end. This activity is sustained by a complex protein cap that stabilizes and promotes growth of the microtubule and is lost upon catastrophe or pause and is reformed following initiation of growth (Mimori-Kiyosue, 2003). Understanding this complex system is critical not only for understanding the basis of a wide array of cellular processes, but is also very relevant clinically, as many of the most successful chemotherapeutic drugs target microtubules (Rinsinger, 2009). However, many of these drugs, such as taxol, have quite deleterious side-effects and developing safer and specific drugs is currently an actively pursued topic. Achieving this can only be done with a complete understanding of the underlying network governing microtubule dynamics regulation.

Tracking Microtubules

In past years, microtubules were tracked using dyes or, more recently, using GFP-labeled tubulin by eye (Goodson, 2010). This is not an optimal solution, as most visualization must occur at the sparse cell edge, as the cellular bulk is densely populated with microtubules and is difficult to distinguish and follow an individual growth. This is solved by instead labeling one of the plus-end-binding proteins with GFP (Tirnauer, 2002; Piehl, 2004). The GFP-labeled cap, typically of EB1 or EB3 (shown in Figure 1.1B), forms as an oval mass, earning them the name of 'comets' due to their shape and movement in videos. This comet is on the growing end and is lost upon catastrophe and can readily be followed by eye. Using a protein complex that only forms on growing microtubules has its own limitations, as microtubules are essentially invisible during shrinkage and pausing. However, with careful consideration, this can be solved. By using algorithms that can predict possible trajectories of growth and shrinkage upon loss of a comet

based on prior movement, catastrophe, rescue and pause events can be detected. Manual tracking is, however, prone to overestimating growth rates, by simple human bias towards detecting the most obvious events. Tracking comets can be massively up-scaled and reliably tracked through the use of automated tracking programs that can identify, follow and analyze the movement of comets (Matov, 2010; Applegate, 2011). plusTipTracker, developed by Applegate et al. and the Danuser Lab is one such program and is dispersed freely by the Danuser Lab and, due to its ease of use and robust and reliable tracking (Applegate, 2010), will be used in this study to analyze microtubule dynamics in two models. The first condition will be the relation between stathmin, a known regulator of microtubules, and p27, a classic cell cycle checkpoint protein. The second condition will be the relationship between taxol, a microtubule stabilizing drug and p53, a DNA-damage checkpoint protein.

Stathmin, A Microtubule Regulator

Stathmin, or oncoprotein 18, is a small, known microtubule binding protein (Belmont, 1996) and has a well-characterized effect on microtubules. The C-terminal end of stathmin can bind and sequester 2 tubulin subunits, while the N-terminal end is capable of binding to microtubules and promoting catastrophe (Howell, 1999a) and is known to regulate global microtubule dynamics in interphase (Howell, 1999b; Sellin, 2008; Ringhoff and Cassimeris, 2009). Despite its small size, it is known to have many effects on cells far beyond that of its tubulin-sequestering abilities and is responsible for proper recruitment of Plk1 and Aurora A to the centrosome and timely transition into mitosis (Silva, 2013). As microtubules are instrumental in the proliferation and metastasis of cancers, stathmin is commonly over-expressed in a variety of cancers (Brattsand, 2000). A known binding partner to stathmin is p27, a cyclin-dependent kinase inhibitor typically implicated in the G1 checkpoint (Boehm, 2002), but with additional roles in cell migration, differentiation and RhoA signaling (Nguyen, 2006). p27 was found to bind to C-terminal end of stathmin, negating its tubulin sequestering capabilities while leaving its catastrophe-promoting capabilities intact (Baldassarre, 2005; Belletti, 2010). Given both proteins roles in cells, understanding the consequences of their interactions could provide potential mechanisms or targets for future drugs discovery.

Taxol, p53 and Microtubules

p53 has been called 'the guardian of genome' since it plays such a critical role in the DNA-damage response pathway. Because of this critical function, it is commonly found lost or nonfunctional in cancers (Baroni, 2004). Following severe DNA damage, p53 is phosphorylated and transported into the nucleus, where it acts as a transcription factor, capable of promoting cell death (Moll, 2001). p53, however, is able to alter a wide variety of cell functions, of particular interest is its ability to modify microtubule dynamics (Murphy, 1996; Galmarini, 2003) and has been proposed to regulate microtubule dynamics through its transcriptional downregulation of microtubule stabilizers such as STOP and MAP4, increasing dynamic instability (Murphy 1996; Zhang, 1998; Galmarini, 2003). However, the relationship between microtubule stabilizers and p53 would appear to be quite complex and dynamic, as MAP4 has also been found to be upregulated in the presence of p53 (Galmarini, 2003). As p53 transport to the nucleus is dependent on dynein motors (Giannakakou, 2002), it would seem that promoting microtubule stability through drugs such as the taxanes would enhance p53 transport and subsequently initiate apoptosis (Giannakakou, 2002). However, there is no clear consensus on what effect p53 status has on taxol treatments, with some reports claiming p53-independence (Bacus, 2001), loss of p53 promoting cell death (Wahl, 1996), and presence of p53 promoting death (Tan, 2002). This apparent contradiction may be cell-type dependent, and may arise from the mechanism or timing of death in these cells.

Initially, taxol treatment to cells was thought to kill by arresting cells at the G2/M transition by not allowing microtubules to depolymerize (Milas, 1995). However, these concentrations were found to be nearly 100 times that found in actual treatment cells (Yeung, 2000). In these lower concentrations, around 5-10 nM, cells progressed into mitosis, but ultimately stalled, and later died by apoptosis (Jordan, 1997). It is not clear if the aneuploidy and micronuclei observed following mitotic exit were a result or cause of apoptosis from aberrant spindle dynamics or if taxol activated a cryptic apoptotic pathway (Bacus, 2002). With both p53 and taxol affecting microtubules, it is alluring to suggest that cell death is activated by a microtubule-dependent process. With the newly gained ability to detect minute variations in microtubule dynamics with automated tracking programs like plusTipTracker, we hope to elucidate how taxol affects

microtubule dynamics and how that response may differ in the presence or absence of p53 and if this affects when either type of cell dies. If p53-deficient cells respond differently, it may be possible to design therapies to target these mechanisms or pathways more effectively, with the goal of minimal damage to healthy cells. For example, a combined treatment of a low dosage of taxol with a drug that targets the cell cycle stage in which p53-deficient cells die may act in synergy to kill cancerous cells with little toxicity to p53-expressing, healthy cells.

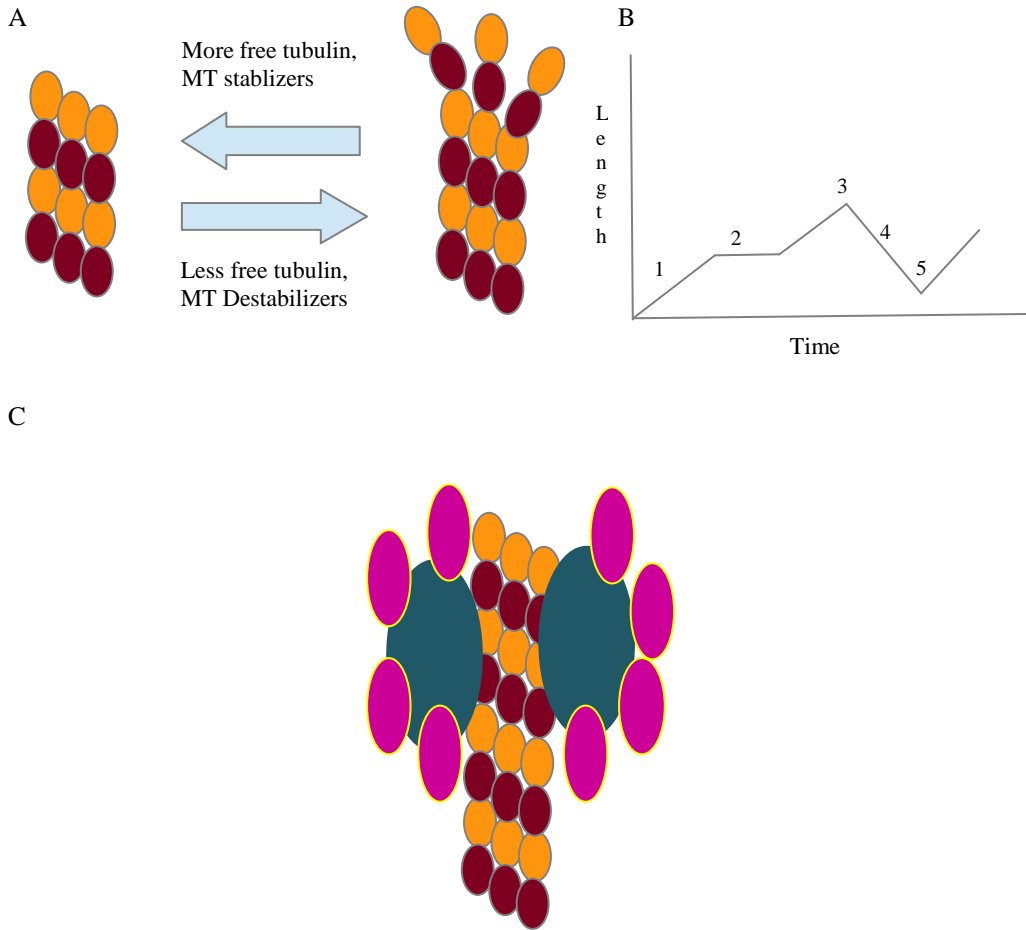
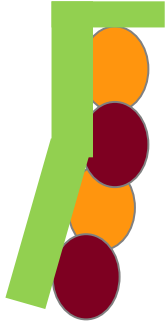


Figure 1: Microtubule Dynamics and Comet Structure. (A) Microtubules are composed of a ring of 13 subunits of α - (orange) and β - (brown) tubulin. For simplicity, only 3 were shown. Microtubules can grow and shrink, exhibiting dynamic instability, the switching between growth and shrinkage without influence, but the balance between the two can be affected by a variety of proteins. A schematic of growth showing growth (1), pause (2), catastrophe (3), shortening (4) and rescue (5) (B). A simplified cartoon of a plus-tip protein cap, or comet. Tubulin-orange/brown, EB1-blue, EB3-pink (C).

A



B

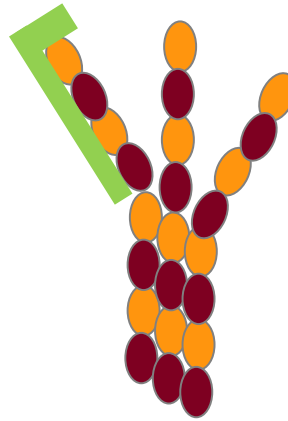


Figure 2: Mechanism of Stathmin Regulation of Microtubules in Cells. The C-terminal end of stathmin and the helical backbone, the T2S region, can bind and sequester 2 tubulin subunits in a kinked fashion (A), while the N-terminal end is capable of binding to microtubules and promoting catastrophe (B). The N-terminus is a hook-shaped extension that binds to plus ends of α -tubulin. This causes stathmin to bind to the end of microtubules and force the kinked binding structure, promoting catastrophe. Later diagrams show a simplified version without the kink in the tubulin-stathmin complex. Stathmin is shown in green, tubulin subunits are shown in orange/brown. (Howell, 1999; Steinmetz, 2007, Goodson, 2012).

Results

Establishing and Determining a Standard plusTipTracker Procedure

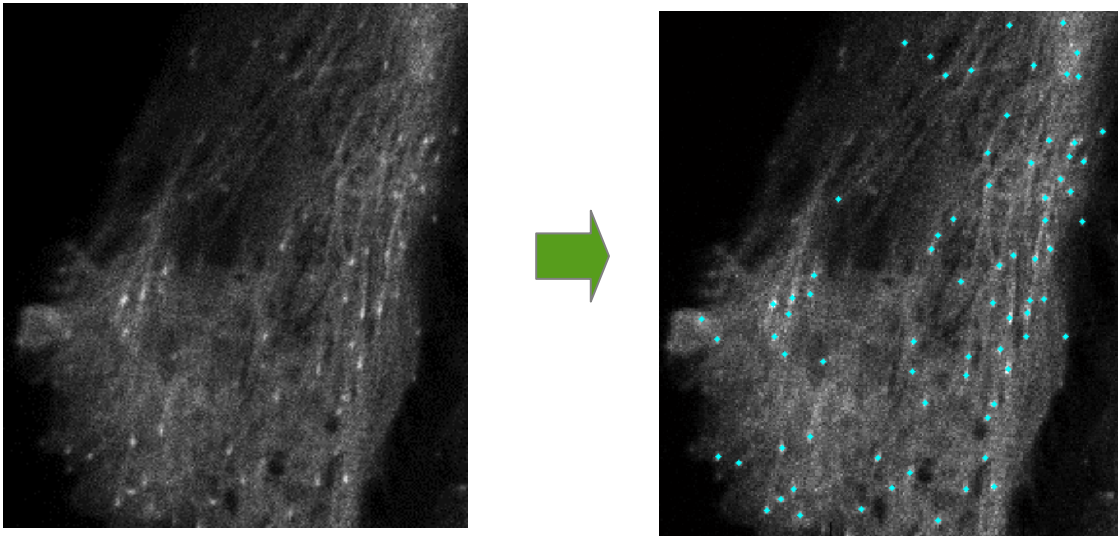
plusTipTracker uses several parameters to detect and analyze microtubule dynamics; these are: Comet size, a minimum and maximum size for intensity; time window, the amount of time a comet can disappear and reappear and still be considered the same track; forward and backward angles, to detect catastrophe and predict paths; shrinkage factor, to detect maximum catastrophe length; and fluctuation radius, to account for movement while in very slow growth or pause. Since microtubule dynamics are heavily influenced by cell type and environment, it is necessary to determine what parameters plusTipTracker will use for a standardized detection and analysis in a variety of conditions with a prior untested but common cell line, HeLa cells. A representative still image is shown illustrating the plusTipTracker software detecting comets in Figure 2A.

As comet size is a product of microtubule structure, measurements from still images (2B) reveal that most comets tend to range between minimum 4 pixels to maximum 10 pixels (figure 3), which, after using the integrated scaling software, equals roughly 0.6 to 1 microns in diameter in length. This mirrors previous dimensions (Applegate, 2010) for this. As microtubule bending is constrained by the physical nature of the structure, a maximum forward angle of 30° and a maximum backward angle of 10° was chosen as per prior reports (figure 4). Shrinkage factor and fluctuation radius do not influence the results noticeably, so the prior usage of 1.5 and 2.0, respectively, were used (figure 5). Time window was determined by varying this setting and seeing when the number of pause events begins to plateau. Once again, our average time window of 13 secs (figure 6) is very similar prior findings of 12 seconds (Applegate, 2010). Representative graphs for the impact of parameter variance are shown in the figures 3-6. It is important to note that most parameters do not heavily impact the resulting output. plusTipTracker has been shown to be robust and largely parameter-independent, leaving less chance that results may be influenced by incorrectly determined parameters. Regardless, more conservative values allow for more true events to be detected and to eliminate false positives. Developing a standardized parameter set will allow for confident large-number evaluation of experimental variables such as altered levels of microtubule regulators or drug incubation, both of which are utilized here. For a more detailed description of the roles of various

parameters and detection algorithms used by plusTipTracker, see the technical report included in the software package (Applegate 2010)

Individual comet tracks were collected and analyzed from metadata generated by plusTipTracker. Cell analysis was divided into two general regions: the cell periphery, or cell edge, is defined as 5 microns in from the edge of the cell membrane; the cell bulk is the remaining visible area. For a given track to belong in a either area, it must spend the majority (>60%) of its lifetime in that area. When used on control-treated cells (DMSO or non-targeting siRNA), the resulting statistics on dynamics is in correspondence with previously reported dynamics (Odde, 1995, Applegate 2011). This is shown in table 1 and is used for comparison in all further experiments. While we did not find any difference between cell periphery dynamics and cell bulk dynamics as previously reported (Matov, 2010; Applegate, 2010; Applegate, 2011), this can be attributed to using different cells lines, as our cell line of interest, HeLas, has not been analyzed previously.

A



B

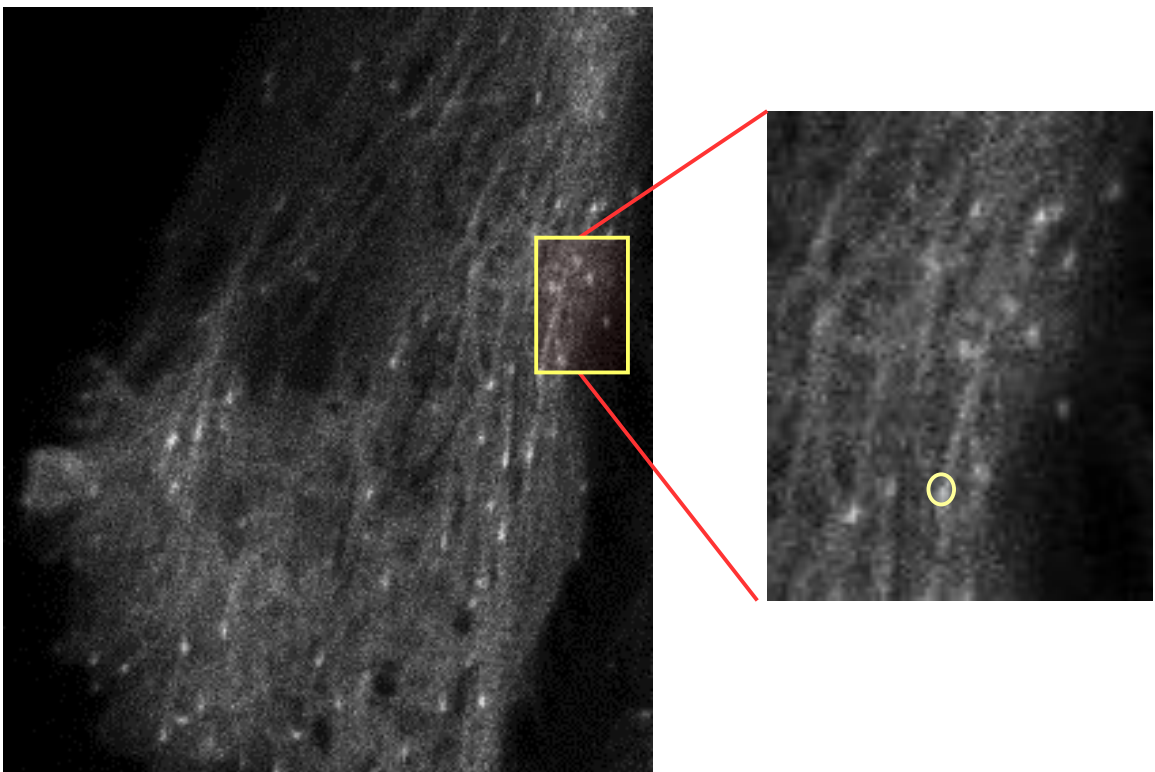
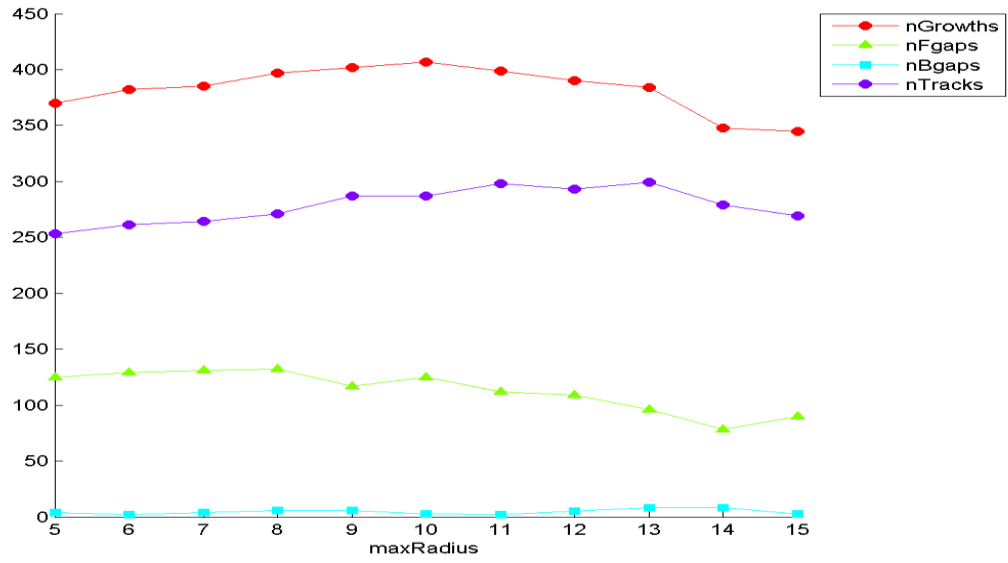


Figure 3: Comet Detection and Size. plusTipTracker accurately detects comets based on relative brightness (A) and. Determination of the average size of comets was found using scaling software integrated into the the SFC microscope. (B).

A



B

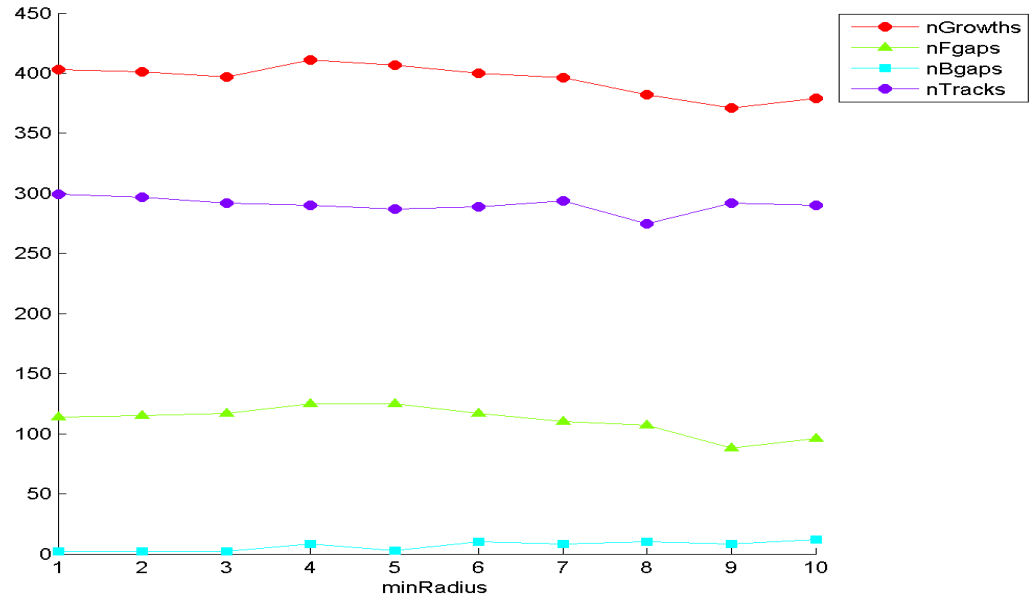
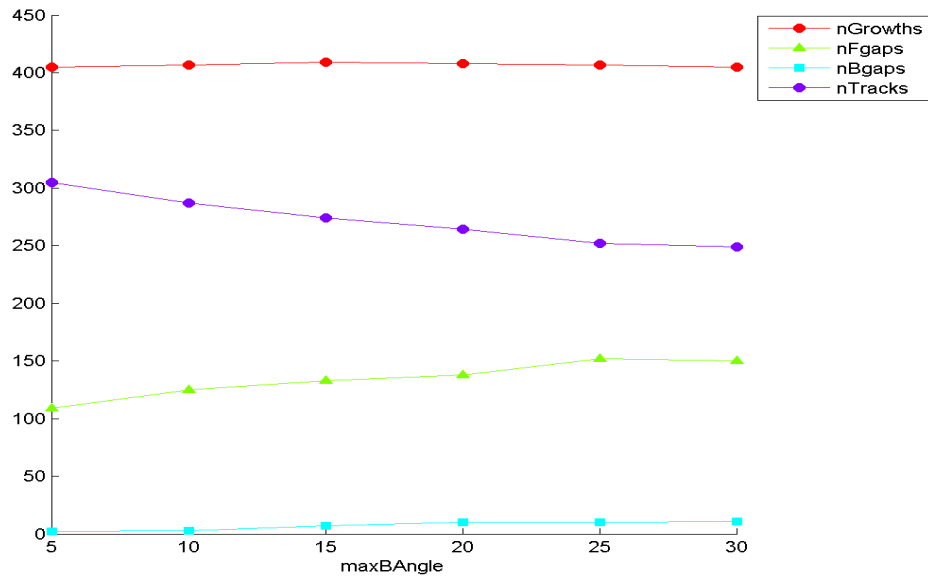


Figure 4: Parameter Determination of search radius. Effect of a value sweep for the minimum comet radius (minRadius, A) and the maximum comet radius (maxRadius, B) on the number of tracks, growths, pauses (Fgap), and rescue events (Bgap) on a representative control cell.

A



B

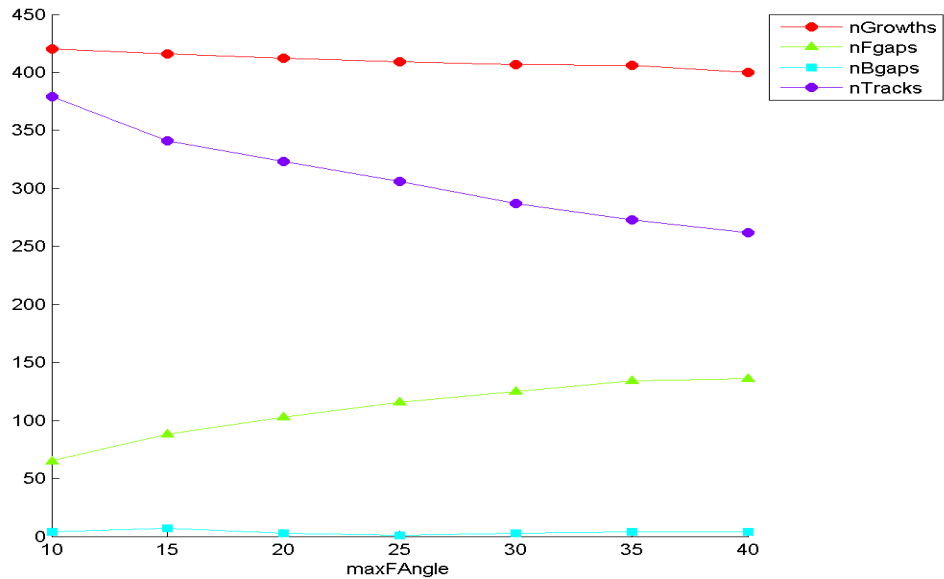
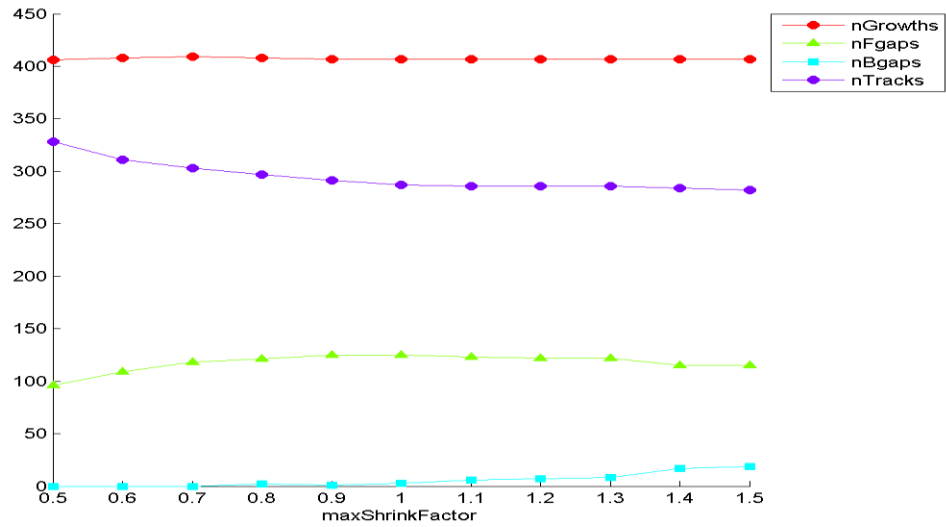


Figure 5: Parameter Determination of Backward and Forward Angles. These parameters are used in Catastrophe events (maxBAngle, A) and predicting paths (maxFAngle, B), respectively and how varying these impacts the number of tracks in growth, pause and shortening. These plateau around 10° and 30° and reflect Applegate's parameter choice and reasoning. Narrower angles allow for less false positives detected or separate tracks linked with little impact on true events, but may reduce rescue detection.

A



B

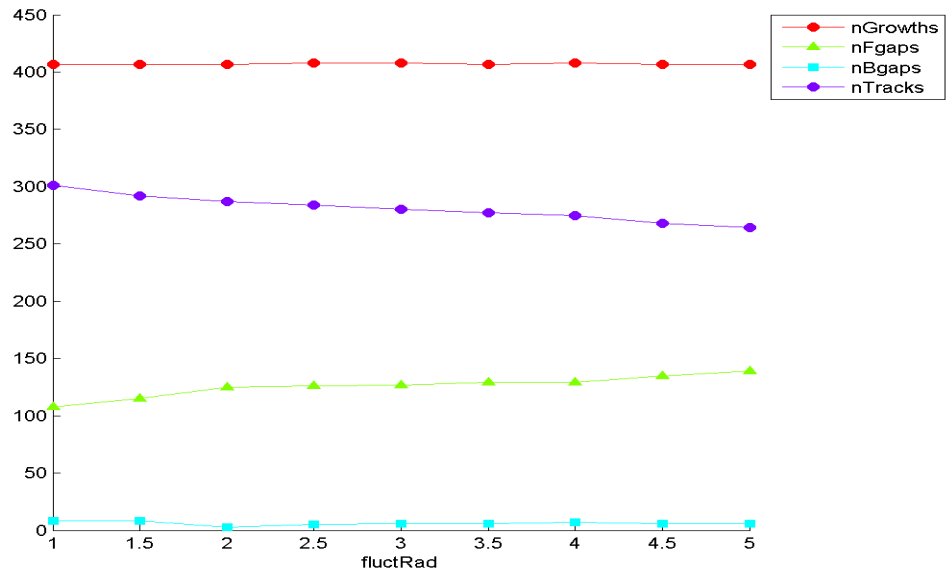


Figure 6: Parameter Determination of Shrinkage Factor and Fluctuation Radius. Shrinkage Factor (maxShrinkFactor, A) sets a maximum shortening rate as a factor of growth rate and length to minimize false catastrophe events. Fluctuation Radius (fluctRad, B) restricts how far a paused comet can drift before it will be considered a new track. Values of 1.5 and 2.0 were used, as suggested by Applegate.

A

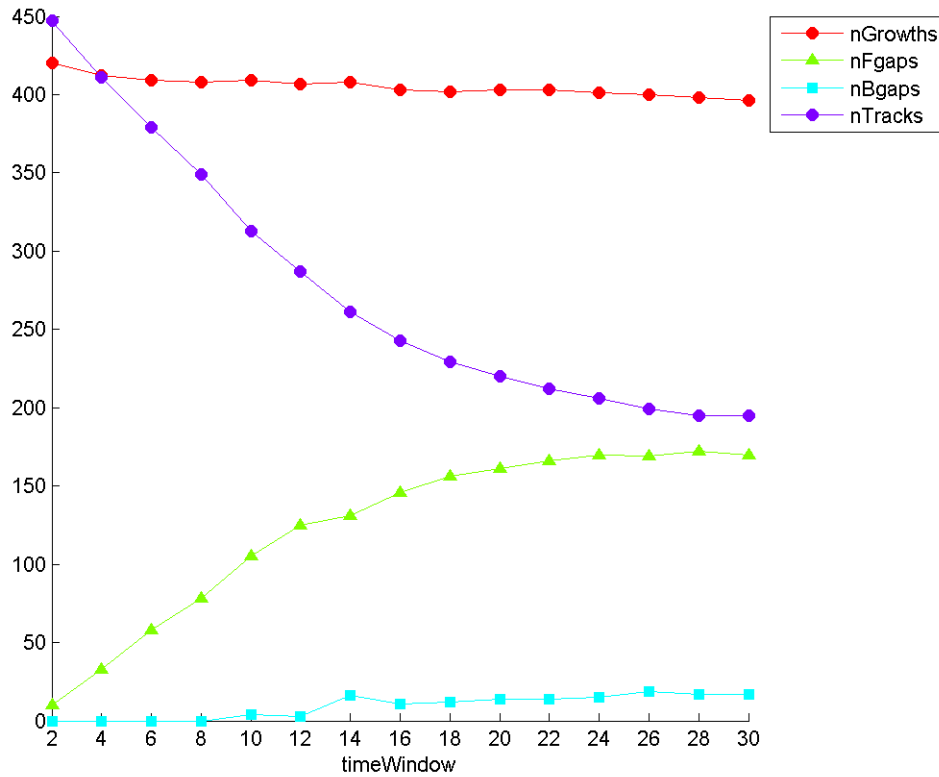


Figure 7: Parameter Determination of Time Window. Time window reflects how long a comet can not be detected in an area (Fluctuation Radius, figure 2.4B) prior to being detected and then be re-detected in said area and still be considered the same track or to shift out of focus, but reappear in the predicted path using the forward angle. A smaller number minimizes the number of false pause, or fGap events, while a larger number allows for more true events of EB1-Comet loss and drifting in and out of the plane of focus events to be detected. Following Applegate's value of 12 seconds, we found a plateau in fGap (pause events) around 12-14 seconds and subsequently used this as our standard time window value.

	Cell edge	Cell Bulk
Growth Rate ($\mu\text{m}/\text{min}$)	21.07 ± 3.75	20.38 ± 2.99
Growth lifetime (sec)	9.23 ± 1.28	9.40 ± 1.50
Growth Length (μm)	3.078 ± 0.682	2.99 ± 0.671
Pause Lifetime (sec)	13.99 ± 2.14	14.32 ± 2.35
Pause Rate per Minute	$0.151 \pm .0284$	0.149 ± 0.0422
Pause Rate per Micron	0.565 ± 0.201	0.716 ± 0.731
Shortening Rate ($\mu\text{m}/\text{min}$)	38.42 ± 7.78	38.58 ± 7.76
Shortening Lifetime (sec)	6.57 ± 1.91	6.85 ± 2.04
Shortening Length (μm)	4.13 ± 1.36	4.21 ± 1.67
Rescue Rate per Minute	0.129 ± 0.069	0.128 ± 0.0780
Rescue Rate per Micron	0.391 ± 0.227	0.455 ± 0.339
Catastrophe Rate per Minute	0.160 ± 0.0164	0.160 ± 0.0165
Catastrophe Rate per Micron	0.746 ± 0.367	0.746 ± 0.306
Percent Time Spent in Growth	73.90 ± 8.48	76.9 ± 8.49
Percent Time Spent in Pause	24.7 ± 8.38	21.8 ± 7.75
Percent Time Spent in Shortening	1.40 ± 1.35	1.26 ± 1.58

Table 1: Microtubule Dynamics of DMSO-treated/non-targetting siRNA Transfected Cells. No significant differences were found between the cell edge and bulk. (N=49) No significant difference was found between untreated, DMSO-treated, or non-targetting siRNA transfected HeLa cells. (not shown) These numbers are similar to previous reports using similar cell types (Odde, 1995; Matov, 2010, Applegate, 2011). While we did not see differences in dynamics between these two groups, this can be attributed to different cell types.

Stathmin and p27

Effects of Stathmin Depletion on MT Dynamics

Stathmin is known to regulate microtubule dynamics by sequestering tubulin subunits on its C-terminal end and promoting catastrophe on its N-terminal end (Cassimeris, 2002), and should provide a readily visible phenotype to provide additional verification of the utility of the plusTipTracker. To elucidate the effects of stathmin on microtubule dynamics in our *in vivo* setting, stathmin was depleted by using siRNA knockdown (KD) and confirmed by western blot (2A). Cells were fixed and imaged to ensure that comets were not affected by knockdown (figure 9). Stathmin-depleted cells' microtubule dynamics are reported in table 2A. It is interesting to note that shortening length and lifetime are decreased in the cell edge, indicating that these cells have a less dynamic microtubule skeleton. When compared to control cells (table 2B), there is an increase in growth rate and length, due to depletion of a tubulin-sequestering protein, concomitant with a decrease in catastrophe, as expected. While these changes were not as pronounced as expected, earlier findings indicate that stathmin has a relatively minor effect on dynamics, and has little effect on the cellular periphery dynamics (Ringhoff, 2009). Our findings corroborate this by showing that there is no change in the dynamic turnover of microtubules at the cellular periphery, but shows the proposed increased growth rate and increased catastrophe rate in the cellular bulk, an area previously not visualized or characterized. Additionally, other microtubule regulators may be able to buffer some effects following the loss of a key regulator, as cells would have ample time to adjust to a new steady state.

Effects of p27 Depletion on MT Dynamics

We next investigated the potential role of p27 in microtubule dynamics. p27 did not alter comet number (figure 9). Following depletion of p27, microtubules in the cell bulk became more stable and long-lived, without any increase in other global dynamics (table 3A). When compared to control cells, p27-depleted cells have shorter growth lengths and lifetimes, in addition to increased pausing (table 3B). This would seem to suggest that microtubules have been made much less stable and less free tubulin is available. It is interesting to note that this increase in growth stability is independent of any change in catastrophe or rescue rate and only occurs in the cell edge. In contrast to that, shortening rate is decreased, which would suggest increased stability.

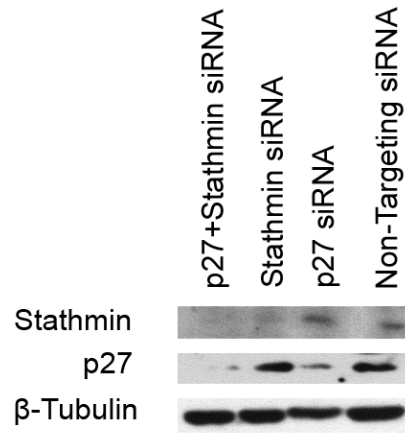
As p27 is involved in many cell migration functions (Baldassarre, 2005), this could explain the constrained area of change. The exact cause of this change is difficult to pin down, as p27 affects a large number of pathways, many of which have proteins that alter the cytoskeleton, and may create complex changes in microtubule dynamics (Song, 2001; Godin, 2012). An additional factor may be localization and stability of p27, as some cells may have most p27 kept inside the nucleus or rapidly degrade cytosolic p27, limiting its potential effects on microtubules (Ishida, 2007).

p27/Stathmin Interaction and Co-depletion

As p27 is a known binding partner to stathmin (Baldassarre, 2005) once in the cytosol, it seemed tempting to suggest that the decreased stability-phenotype we see in p27-depleted cells is due to release of bound stathmin. If p27's effects on microtubules is independent of stathmin, then a knockdown of both proteins should produce an additive profile, having the stathmin knockdown's increased catastrophe dynamics and the p27 knockdown's increased growth stability and increased pausing. An additional test would be a comparison against the prior knockdowns. Independent effects should have equal dissimilarity to the other depletion. However, if p27 regulates microtubules predominately through locking up stathmin, a co-depletion of both proteins should appear most like the stathmin knockdown. Knockdown of both p27 and stathmin did not affect comets (figure 9). Co-depletion caused a reduction in shortening length and lifetime in the cell edge, but with increased catastrophe frequency when compared to the cell bulk (table 4A). When this co-depletion was compared to control cells, most differences seen were in identical qualities as seen with with stathmin depletion, such as increased growth stability and decreased catastrophe frequency (table 4B). When these values were compared with the other two conditions, comparing p27 depletion resulted in many groups becoming significant with increased growth stability and increased growth rate, possibly from increased free tubulin. This co-depletion, then, could be simplified as a low stathmin to high stathmin comparison, and this model fits well given this data. However, when compared to stathmin depletion, only one parameter had increased, growth length.

Given all of these findings, p27 could be exerting its microtubule regulation by proxy, through locking up free stathmin and replicating, to a much less extent, artificial depletion of stathmin by competing with tubulin. As these cells have had over 24 hours since depletion, it is unknown if the profiles generated reflect steady-state dynamics or recent loss of protein. The sole significant group when comparing stathmin depletion to co-depletion, growth length, could be a result of an affected pathway from loss of p27. It is important to note that cytosolic concentrations of p27 can be quite low, especially in many types of cancer (Besson, 2004). It is currently not clear how large of a role p27-stathmin interaction plays any role in microtubule dynamics in healthy cells (Bettelli, 2010), but may influence microtubule dynamics in cancers that have either lost p27 or over-expressed stathmin. As a proof by example, plusTipTracker was able to derive at an identical model of p27-stathmin interaction that was established prior to this work, but solely through dynamics analysis, highlighting its power in analysis and capability as a tool. As this is liable to misinterpretation or various cellular responses or mechanisms to compensate for protein loss, additional experiments would be needed to verify any conclusions.

A



B

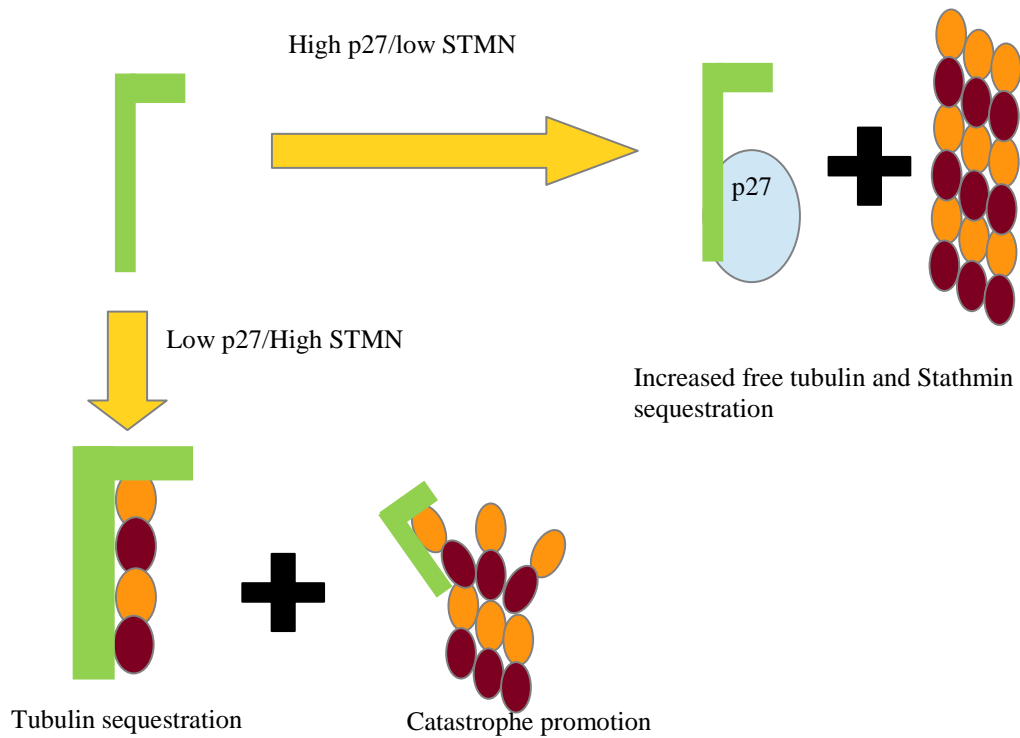


Figure 8: p27/Stathmin Influences Microtubule Dynamics. A Western blot for p27, Stathmin (STMN), and p27+Stathmin knockdowns (A). The blot was re-probed for β -tubulin as a loading control between all lanes to ensure equal loading of protein. A possible model for how p27/Stathmin influences microtubule

dynamics (B). p27 exerts regulation of microtubules through stathmin by competing for tubulin binding sites. Stathmin -Green, Tubulin Dimer – Orange/Brown, p27 – Blue.

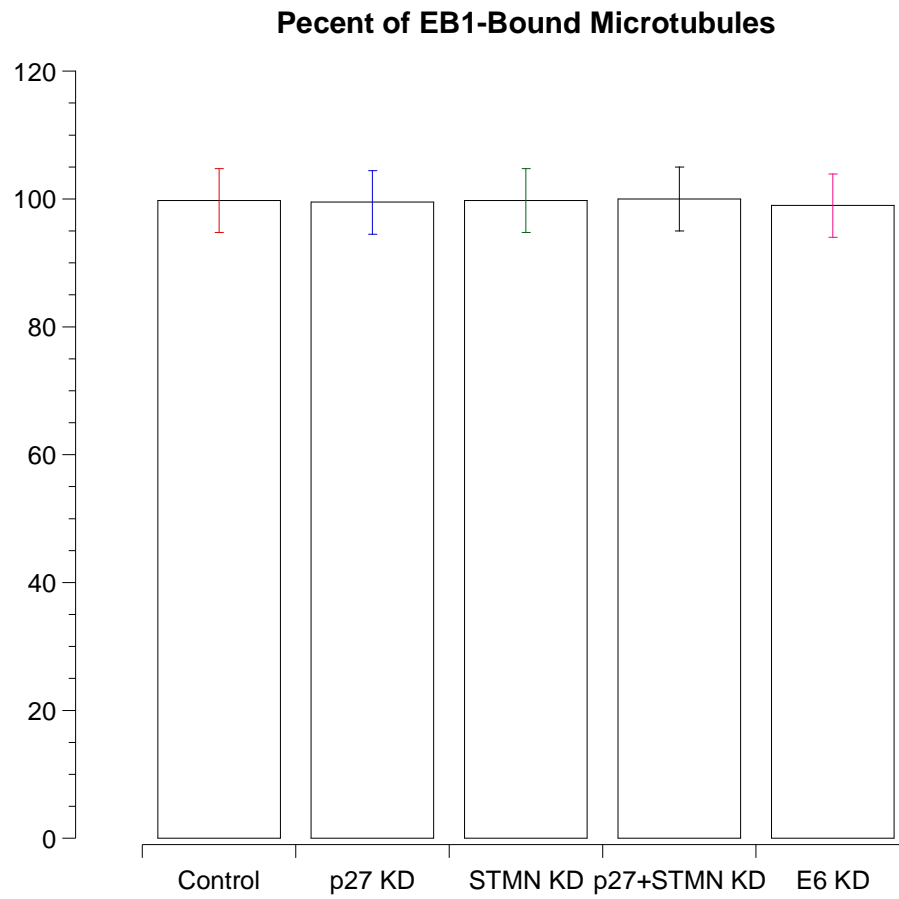


Figure 9: Experimental Conditions do not Affect Comets. No experimental condition used was found to change comet number. Comets were visualized with EB1-GFP. Tubulin was visualized with immunofluorescence (Carney and Cassimeris, 2010). Three replicates were counted and percent of microtubules with a comet present was collected.

A

	Cell Edge	Cell Bulk
Growth Rate ($\mu\text{m}/\text{min}$)	21.37 ± 2.58	21.61 ± 2.40
Growth lifetime (sec)	9.51 ± 1.39	9.99 ± 1.25
Growth Length (μm)	3.18 ± 0.514	3.40 ± 0.581
Pause Lifetime (sec)	13.46 ± 1.92	14.13 ± 1.65
Pause Rate per Minute	0.157 ± 0.0197	0.155 ± 0.0187
Pause Rate per Micron	0.572 ± 0.166	0.5916 ± 0.206
Shortening Rate ($\mu\text{m}/\text{min}$)	38.27 ± 5.53	38.28 ± 4.94
Shortening Lifetime (sec)*	6.58 ± 1.34	7.31 ± 1.61
Shortening Length (μm)*	4.099 ± 0.771	4.55 ± 1.07
Rescue Rate per Minute	0.127 ± 0.0599	0.139 ± 0.0600
Rescue Rate per Micron	0.558 ± 0.742	0.523 ± 0.303
Catastrophe Rate per Minute*	0.160 ± 0.0130	0.154 ± 0.00962
Catastrophe Rate per Micron	0.702 ± 0.153	0.706 ± 0.120
Percent Time Spent in Growth	75.74 ± 7.43	75.39 ± 6.58
Percent Time Spent in Pause	22.94 ± 7.08	22.9 ± 5.47
Percent Time Spent in Shortening	1.30 ± 0.92	1.69 ± 1.64

B

	Bulk	Edge
Growth Rate	+6.01*	-
Growth Lifetime	-	-
Growth Length	+13.6**	-
Pause Lifetime	-	-
Pause Rate per Minute	-	-
Pause Rate per Micron	-	-
Shortening Rate	-	-
Shortening Lifetime	-	-
Shortening Length	-	-
Shortening Rate per Minute	-	-
Shortening Rate per Micron	-	-
Catastrophe Rate per Minute	-4.1*	-
Catastrophe Rate per Micron	-13.0*	-
Percent Time in Growth	-	-
Percent Time in Pause	-	-
Percent Time in Shortening	-	-

Table 2: Dynamics of Stathmin-Depleted Cells. Table 2A lists the dynamics in Stathmin KD Cells (N=36) and compare the cellular bulk to the cell edge. Table 2B compares these respective values to those of control cells, with the difference in percent change. * denotes $p < 0.05$, ** denotes $p < 0.01$. Boxes marked with a dash or no * had no significant difference.

A

	Cell Edge	Cell Bulk
Growth Rate ($\mu\text{m}/\text{min}$)	20.01 \pm 2.20	19.64 \pm 3.00
Growth lifetime (sec) **	9.25 \pm 1.08	9.89 \pm 1.14
Growth Length (μm) ***	2.27 \pm 0.385	3.01 \pm 0.610
Pause Lifetime (sec)	12.9 \pm 2.34	13.9 \pm 2.13
Pause Rate per Minute	0.156 \pm 0.0180	0.148 \pm 0.0320
Pause Rate per Micron	0.656 \pm 0.191	0.619 \pm 0.236
Shortening Rate ($\mu\text{m}/\text{min}$)	34.53 \pm 6.25	35.03 \pm 4.93
Shortening Lifetime (sec)	7.04 \pm 1.54	7.84 \pm 2.06
Shortening Length (μm)	3.96 \pm 1.08	3.96 \pm 1.19
Rescue Rate per Minute	0.135 \pm 0.0595	0.120 \pm 0.0715
Rescue Rate per Micron	0.464 \pm 0.275	0.432 \pm 0.322
Catastrophe Rate per Minute	0.159 \pm 0.0137	0.154 \pm 0.0162
Catastrophe Rate per Micron	0.779 \pm 0.506	0.797 \pm 0.232
Percent Time Spent in Growth	76.22 \pm 7.4	76.44 \pm 8.95
Percent Time Spent in Pause	21.98 \pm 7.35	21.9 \pm 7.35
Percent Time Spent in Shortening	1.76 \pm 1.41	1.65 \pm 1.73

B

	Bulk	Edge
Growth Rate	-	-
Growth Lifetime	-	-
Growth Length	-	-26.6***
Pause Lifetime	-	-6.5*
Pause Rate per Minute	-	-
Pause Rate per Micron	-	+12.9*
Shortening Rate	-	-10.2*
Shortening Lifetime	-	-
Shortening Length	-	-
Shortening Rate per Minute	-	-
Shortening Rate per Micron	-	-
Catastrophe Rate per Minute	-	-
Catastrophe Rate per Micron	-	-
Percent Time in Growth	-	-
Percent Time in Pause	-	-
Percent Time in Shortening	-	-

Table 3: Dynamics of p27-Depleted Cells. Table 3A lists the dynamics in p27 KD Cells (N=34) and compare the cellular bulk to the cell edge. Table 3B compares these respective values to those of control cells, with the difference in percent change. * denotes $p < 0.05$, ** denotes $p < 0.01$, *** denotes $p < 0.001$. Boxes marked with a dash or no * had no significant difference.

A

	Cell Edge	Cell Bulk
Growth Rate ($\mu\text{m}/\text{min}$)*	20.01 ± 2.08	21.02 ± 2.23
Growth lifetime (sec) *	10.2 ± 1.20	9.49 ± 1.39
Growth Length (μm)	3.17 ± 0.44	3.12 ± 0.53
Pause Lifetime (sec)	13.8 ± 1.4	13.69 ± 1.81
Pause Rate per Minute	0.150 ± 0.0115	0.157 ± 0.0204
Pause Rate per Micron	0.671 ± 0.414	0.608 ± 0.156
Shortening Rate ($\mu\text{m}/\text{min}$)	35.4 ± 5.4	37.4 ± 13.6
Shortening Lifetime (sec)	6.42 ± 1.01	6.86 ± 1.68
Shortening Length (μm)	4.21 ± 0.722	3.96 ± 1.28
Rescue Rate per Minute	0.158 ± 0.0602	0.130 ± 0.0737
Rescue Rate per Micron	0.535 ± 0.393	0.569 ± 0.516
Catastrophe Rate per Minute	0.153 ± 0.0102	0.159 ± 0.0147
Catastrophe Rate per Micron	0.720 ± 0.130	0.711 ± 0.144
Percent Time Spent in Growth	76.5 ± 6.01	77.0 ± 6.4
Percent Time Spent in Pause	22.6 ± 5.65	22.2 ± 6.06
Percent Time Spent in Shortening	0.991 ± 0.778	0.78 ± 0.65

B

Compared to...	To control		To STMN KD		To p27 KD	
	Bulk	Edge	Bulk	Edge	Bulk	Edge
Growth Rate	-	-	-	-	7.08*	-
Growth Lifetime	-	+9.73***	-	7.25*	-	12***
Growth Length	-	-	-	-	-	39.6*
Pause Lifetime	-	-	-	-	-	6.47*
Pause Rate per Minute	-	-	-	-	-	-
Pause Rate per Micron	-	-	-	-	-	-
Shortening Rate	-	-	-	-	-	-
Shortening Lifetime	-	-	-	-	-	-
Shortening Length	-	-	-	-	-	-
Shortening Rate per Minute	-	-	-	-	-	-
Shortening Rate per Micron	-	+36.7*	-	-	-	-
Catastrophe Rate per Minute	-	-3.9*	-	-	-	-
Catastrophe Rate per Micron	-	-	-	-	-	-
Percent Time in Growth	-	-	-	-	-	-
Percent Time in Pause	-	-	-	-	-	-
Percent Time in Shortening	-	-	-	-	-	-

Table 4: Dynamics of p27- and Stathmin-Depleted Cells. Table 4A lists the dynamics in p27 KD Cells

(N=35) and compare the cellular bulk to the cell edge. Table 4B compares these respective values to those

of control, p27 KD and Stathmin (STMN) KD cells, with the difference in percent change. * denotes

p<0.05, ** denotes p<0.01, *** denotes p<0.001. Boxes marked with a dash or no * had no significant difference

Taxol and p53

Effects of p53 Restoration of MT Dynamics

p53's role in microtubule dynamics has not been clear, partly due to its wide-reaching effects on a variety of cellular pathways. We therefore set out to characterize how restoring p53 in a p53-deficient cell line, the HeLas (Hoppe-Seyler, 1991) would alter microtubule dynamics. Transfection with the E6 siRNA restored p53 levels, though the activity, localization and phosphorylation of p53 was not tested (figure 4), though it is likely p53 is transcriptionally active (Goodwin, 2000). After restoring p53, microtubule dynamics were characterized (table 5A) in interphase cells, since individual microtubule ends and comets are easier to resolve than when they are in the dense mitotic spindle. When compared to the historic p53-deficient cells, microtubules displayed decreased shortening dynamics, reduced catastrophe, and increased growth stability (table 5B). Similar to the effect of stathmin, most changes were rather small. How these effects are achieved is not clear, though this may be in part due to upregulation or downregulation of transcriptional targets. This decrease in dynamicity reflects previous findings that p53 stabilizes microtubules to aid in its nuclear transport following activation (Giannakakou, 2002). This finding provides a possible mechanism of p53-enhanced death following taxol treatment by allowing more efficient transport of p53 to the nucleus (Tan, 2002; Giannakakou, 2002).

Effects of 10 nM Taxol Treatment on MT Dynamics

We then set out to characterize the effect of physiological concentrations of taxol during typical treatments. After allowing p53-deficient cells four hours of incubation 10 nM solution of taxol to equilibrate between extracellular and intracellular concentrations, dynamics were measured (table 6A). In contrast to all knockdown experiments, taxol treatment resulted in rather prominent changes (table 6B). These results are in agreement with a stabilizing drug's effect on the growing population of microtubules, causing large decreases in growth rate and length, increased pausing or very slow growth, decreased shortening dynamics with increased rescue rates. Curiously, catastrophe rate also increased, but it is not clear why. Overall, though, microtubules were made much more stable. These effects were largely confined to the edge of cells.

Double Treatment of p53 Restoration and 10 nM Taxol on MT Dynamics

Given the stabilizing effects of low concentrations of taxol on microtubule dynamics, we expected that restoration of p53 would act in concert with taxol treatment. After both restoring p53 and incubating in 10 nM taxol for 4 hours, dynamics were measured (table 7A). These were then compared to their respective control group, p53-restored cells (table 7B). This double treatment produced a profile very similar to that of taxol-treated p53-deficient cells, but with a few key differences. In these cells, growth and shortening dynamics are repressed, with increases in pausing, but these are seen in both the cell edge and bulk, in contrast to taxol's periphery-limited affects seen earlier. Strangely, the presence of p53 acts against taxol's ability to promote rescue, as no change was seen in these cells. p53 would appear to sensitize cells to taxol treatment, most likely through the combined microtubule stabilizing activity. To assess this, we compared p53-deficient cells treated with 10 nM taxol to p53-restored cells treated with 10 nM taxol (table 8A). This revealed that the presence of p53 increases the stabilization of microtubules through more stable growth and diminished catastrophe under taxol treatment. As seen with most cell-intrinsic regulation, these changes were rather small.

A

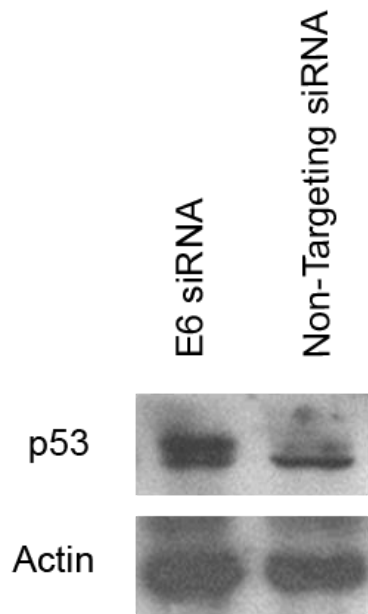


Figure 10: Restoration of p53. p53 is restored by knockdown of the viral protein E6 (A). p53 is located in the middle band of the upper image. The lower band that is in equal intensity in both non-targeting and E6 KD is attributed to non-specific binding of the antibody or to degraded p53. The blot was re-probed with actin to ensure equal loading.

A

	Cell Edge	Cell Bulk
Growth Rate ($\mu\text{m}/\text{min}$)	19.61 ± 2.78	20.62 ± 2.72
Growth lifetime (sec)	10.09 ± 1.27	9.86 ± 1.18
Growth Length (μm)	3.11 ± 0.602	3.19 ± 0.56
Pause Lifetime (sec)	13.49 ± 1.52	13.43 ± 1.80
Pause Rate per Minute	0.153 ± 0.0154	0.152 ± 0.0157
Pause Rate per Micron	0.689 ± 0.351	0.594 ± 0.208
Shortening Rate ($\mu\text{m}/\text{min}$)	36.43 ± 5.78	35.96 ± 5.34
Shortening Lifetime (sec)	6.41 ± 1.46	5.86 ± 1.39
Shortening Length (μm)	3.84 ± 1.01	3.48 ± 0.964
Rescue Rate per Minute	0.158 ± 0.0647	0.146 ± 0.0628
Rescue Rate per Micron	0.536 ± 0.275	0.684 ± 0.731
Catastrophe Rate per Minute	0.152 ± 0.0108	0.158 ± 0.0146
Catastrophe Rate per Micron	0.735 ± 0.159	0.741 ± 0.163
Percent Time Spent in Growth	77.55 ± 6.26	78.79 ± 5.97
Percent Time Spent in Pause	21.01 ± 5.15	20.07 ± 5.51
Percent Time Spent in Shortening	1.44 ± 2.30	1.14 ± 1.65

B

	Bulk	Edge
Growth Rate	-	-
Growth Lifetime	-	+7.9*
Growth Length	-	-
Pause Lifetime	-	-
Pause Rate per Minute	-	-
Pause Rate per Micron	-	-
Shortening Rate	-	-
Shortening Lifetime	-14.6*	-
Shortening Length	-17.0*	-
Shortening Rate per Minute	-	-
Shortening Rate per Micron	-	-
Catastrophe Rate per Minute	-	-4.3*
Catastrophe Rate per Micron	-	-
Percent Time in Growth	-	+5.1*
Percent Time in Pause	-	-15.4*
Percent Time in Shortening	-	-

Table 5: Effect of p53 Restoration on Dynamics. Table 5A lists the dynamics in p53 restored cells (N=33) and compare the cellular bulk to the cell edge. Table 5B compares these respective values to those of

control cells, which are low/depleted p53, with the difference in percent change. * denotes $p < 0.05$, ** denotes $p < 0.01$, *** denotes $p < 0.001$. Boxes marked with a dash or no * had no significant difference.

A

	Cell Edge	Cell Bulk
Growth Rate ($\mu\text{m}/\text{min}$)	17.28 ± 3.48	18.60 ± 3.42
Growth lifetime (sec)	9.68 ± 1.02	9.45 ± 1.19
Growth Length (μm)	2.65 ± 0.684	2.79 ± 0.605
Pause Lifetime (sec)	13.69 ± 1.26	13.72 ± 1.69
Pause Rate per Minute	0.153 ± 0.0160	0.155 ± 0.0184
Pause Rate per Micron	0.767 ± 0.334	0.694 ± 0.264
Shortening Rate ($\mu\text{m}/\text{min}$)	32.85 ± 6.01	32.68 ± 7.83
Shortening Lifetime (sec)	6.42 ± 1.51	6.67 ± 1.99
Shortening Length (μm)	3.47 ± 1.06	3.52 ± 1.20
Rescue Rate per Minute	0.136 ± 0.0699	0.125 ± 0.0690
Rescue Rate per Micron	0.578 ± 0.411	0.552 ± 0.410
Catastrophe Rate per Minute	0.157 ± 0.00885	0.161 ± 0.0136
Catastrophe Rate per Micron	0.947 ± 0.521	0.796 ± 0.231
Percent Time Spent in Growth	77.2 ± 6.83	78.4 ± 7.34
Percent Time Spent in Pause	21.63 ± 5.87	20.37 ± 6.40
Percent Time Spent in Shortening	1.17 ± 1.43	1.23 ± 1.37

B

	Bulk	Edge
Growth Rate	-8.8**	-18.0***
Growth Lifetime	-	-
Growth Length	-	-13.9***
Pause Lifetime	-	-
Pause Rate per Minute	-	-
Pause Rate per Micron	-	+35.6***
Shortening Rate	-10.7*	-14.5***
Shortening Lifetime	-	-
Shortening Length	-	-15.8*
Rescue Rate per Minute	-	-
Rescue Rate per Micron	-	+47.6*
Catastrophe Rate per Minute	-	-
Catastrophe Rate per Micron	-	+26.8*
Percent Time in Growth	-	+4.5*
Percent Time in Pause	-	-12.4*
Percent Time in Shortening	-	-

Table 6: Effects of 10 nM Taxol Treatment. Table 6A lists the dynamics in a 10 nM Taxol solution (N=41) and compare the cellular bulk to the cell edge. Table 6B compares these respective values to those of

control cells, which were treated with DMSO, with the difference in percent change. * denotes $p < 0.05$, ** denotes $p < 0.01$, *** denotes $p < 0.001$. Boxes marked with a dash or no * had no significant difference

A

	Cell Edge	Cell Bulk
Growth Rate ($\mu\text{m}/\text{min}$)	16.90 ± 2.61	16.24 ± 2.79
Growth lifetime (sec)	10.14 ± 1.06	10.14 ± 1.37
Growth Length (μm)	2.68 ± 0.565	2.65 ± 0.671
Pause Lifetime (sec)	14.21 ± 0.983	13.91 ± 1.20
Pause Rate per Minute	0.154 ± 0.0173	0.152 ± 0.0163
Pause Rate per Micron	0.800 ± 0.236	0.796 ± 0.310
Shortening Rate ($\mu\text{m}/\text{min}$)	32.47 ± 5.42	30.52 ± 5.09
Shortening Lifetime (sec)	5.79 ± 1.44	5.44 ± 0.936
Shortening Length (μm)	3.06 ± 0.776	2.77 ± 0.754
Rescue Rate per Minute	0.144 ± 0.0683	0.119 ± 0.0517
Rescue Rate per Micron	0.556 ± 0.284	0.555 ± 0.378
Catastrophe Rate per Minute	0.152 ± 0.00809	0.152 ± 0.0119
Catastrophe Rate per Micron	0.847 ± 0.192	0.972 ± 0.659
Percent Time Spent in Growth	77.27 ± 4.69	77.33 ± 4.02
Percent Time Spent in Pause	22.04 ± 4.39	21.94 ± 3.84
Percent Time Spent in Shortening	0.689 ± 0.654	0.720 ± 0.543

B

	Bulk	Edge
Growth Rate	-18.1***	-18.0***
Growth Lifetime	-	-
Growth Length	-15.7***	-14.1**
Pause Lifetime	+5.9*	-
Pause Rate per Minute	-	-
Pause Rate per Micron	+29.7***	-
Shortening Rate	-10.0*	-17.1***
Shortening Lifetime	-	-14.9***
Shortening Length	-	-28.4***
Rescue Rate per Minute	-	-
Rescue Rate per Micron	-	-
Catastrophe Rate per Minute	-3.9*	-
Catastrophe Rate per Micron	-14.4*	-
Percent Time in Growth	-	-
Percent Time in Pause	-	-
Percent Time in Shortening	-	-

Table 7: Effects of 10 nM Taxol Treatment and p53 Restoration on Dynamics. Table 7A lists the dynamics in a 10 nM Taxol solution with restoration of p53 by E6 KD (N=23) and compare the cellular bulk to the

cell edge. Table 7B compares these respective values to those of p53 restored cells, with the difference in percent change. * denotes $p < 0.05$, ** denotes $p < 0.01$, *** denotes $p < 0.001$. Boxes marked with a dash or no * had no significant difference.

A

	Bulk	Edge
Growth Rate	-9.1*	-
Growth Lifetime	+7.3*	+7.0*
Growth Length	-	-
Pause Lifetime	-	-
Pause Rate per Minute	-	-
Pause Rate per Micron	-	-
Shortening Rate	-	-
Shortening Lifetime	-	-15.2**
Shortening Length	-	-20.4**
Shortening Rate per Minute	-	-
Shortening Rate per Micron	-	-
Catastrophe Rate per Minute	-5.6**	-3.6*
Catastrophe Rate per Micron	-	-
Percent Time in Growth	-	-
Percent Time in Pause	-	-
Percent Time in Shortening	-38.6*	-

Table 8: p53 Restoration Alters Response to Taxol Treatments. Table 8A shows how restoration of p53 alters the microtubule dynamics in response to 10 nM taxol treatment. This compares p53-deficient cells treated with 10 nM taxol to p53-restored cells treated with 10 nM taxol. Changes are shown in percent change. * denotes $p < 0.05$, ** denotes $p < 0.01$, *** denotes $p < 0.001$. Boxes marked with a dash or no * had no significant difference.

Discussion

With the selection of appropriate parameters (figure 2.1-2.5), plusTipTracker is able to reliably and robustly track EB1-GFP comets on microtubule plus ends. Additionally, this process is relatively simple and can be used to develop parameter profiles for a variety of cell types to allow for easy analysis of many known and potential microtubule regulators and drugs, with simple and fast replication in other cells lines. An additional power of this software is the analysis of microtubule dynamics in the cell bulk, an area previously little studied due to the the dense tangle of stable microtubules that occupy this area. This is in stark contrast to previous studies, which focused on relatively few microtubules located in the cell periphery. In total, this project tracked over 200,000 comets and analyzed over 200,000 growth tracks, 130,000 pause events and 40,000 catastrophe and rescue events. The sheer numbers involved allow us to detect minute changes in dynamics that may be constrained to specific areas, such as the leading cell edge in migration or the dense area surrounding a centrosome with great certainty stemming from large- number statistics. Given the sensitivity of cells to changes in microtubule dynamics or protein levels, it is expected that most cell-regulated changes would be small. Additionally, multiple pathways may 'cross-talk', as seen in the p27-stathmin experiments, to act to buffer large changes, allowing a cell to fine-tune its dynamics to fit situations or stages in the cell cycle. It is also interesting that most changes, and most large changes, occur in the cell periphery. The inner network of microtubules may be resistant to change, and disruption of this may be influential in cell viability following drug treatments, as in our study, only taxol was capable of producing large changes in the bulk dynamics.

plusTipTracker does have some caveats, however. As EB1-GFP is used to visualize comets, only the actively growing pool of microtubules are observed. This can be misleading, as overall dynamics could be altered by having more or less microtubules, but would be invisible if only the growing population were tested. Additionally, it is possible the various conditions could remove or diminish comets. This flaw can be resolved if multiple techniques are employed to analyze all populations of microtubules. While these experiments used non-synchronized cells, it remains to be seen if and how dynamics are altered in various stages of the cell cycle, as many regulators are only expressed, localized properly or active during certain

stages of the cell cycle. With the brute-force methods employed here, this should make little difference in the end results, but may underplay the extent of some changes due to 'noise' from inappropriately included cells. Or, if a certain activity is only present for a short duration, such brute-force methods may miss it entirely. Further careful analysis and experimental design should answer these questions.

As a proof-by-example, we attempted to derive a known and characterized interaction through plusTipTracker. For this, we used a protein well studied in our lab: the microtubule destabilizer, stathmin. Stathmin depletion is known to increase actively growing microtubules' stability and may decrease catastrophe *in vivo*. When analyzed by plusTipTracker, we saw exactly that (table 2B). In addition, p27 depletion yields a profile that was the inverse of this, with decreased stability but no change in catastrophe (table 3C). This is expected, as p27 was shown to bind to the C-terminal end of stathmin (Baldassarre, 2005; Godin 2012), an area shown to be involved with its tubulin-sequestering activity but leaving its catastrophe-promoting activity (Howell, 1999; Goodson 2012) functioning in other *in vivo* settings (Baldassarre, 2005; Godin 2012). The double depletion of both proteins yielded a profile very similar to stathmin knockdown, confirming the model suggested by Baldassarre and represented in Figure 8. Interestingly, the double depletion was not a complete recapitulation of stathmin depletion and increased growth lifetime further (table 4B). This highlights the complexity and cross-talk between stathmin and p27, a phenomenon that is likely very common due to the number of microtubule regulators. Here, we provide the first evidence of p27-stathmin regulation in a human cell line. Surprisingly, most changes seen following depletion of either protein were small, ranging from differences of 3 to 15 percent. This is in contrast to *in vitro* studies, which showed that microtubule regulators can produce pronounced effects. This may be the result of cross-talk and buffering by other pathways in order to maintain a consistent, dynamic skeleton. This also makes replicating profiles with various drug treatments problematic, as seen with the dilute taxol treatments, as most drugs produce strong and robust changes.

p53 restoration was seen to have an expected, but small, effect by repressing dynamics (table 5B). As HeLa cells have been deficient in a major DNA-damage checkpoint protein, upon restoration, p53 is likely active

and altering dynamics through transcription (Goodwin, 2000). Similarly, low doses (10 nM) of taxol greatly diminished dynamics, producing the most altered profile yet (table 6B), however, it is interesting to note that this effect was largely constrained to the cell edge, perhaps since this is where the most dynamic microtubules are found. Upon restoration of p53 and treatment with low concentrations of taxol, cells exhibited a greater change in dynamics, having both larger changes and altering bulk dynamics (table 7B). Curiously, p53 abolished the increase in rescue rate seen in taxol treatments alone. It is worthy to mention that this group had the lowest amount of cells, at N=23. This is due to the cells often curling up, presumably to perform apoptosis, soon after imaging, greatly reducing the viable imaging time window. When p53 status was compared between the two taxol treatments, a number of significant changes were seen (table 8A). The presence of p53 caused a further repression of dynamics and catastrophe rate. If taxol-induced death is somehow conveyed through stabilizing microtubules, it is likely that the presence of p53 would sensitize cells to low doses of taxol. This would have implications for both healthy and cancerous cells. However, these changes were relatively small, so p53 status may not influence death at all. Alternatively, the slight increase in microtubule stability may be a signalling method to cells of stress, and this slight increase could more easily activate apoptotic pathways. Further work would need to be done to see if this mechanism is truly a route of activating cell death.

Future Directions and Closing Remarks

Quantifying the nature of cell death following taxol treatment would reveal any potential role microtubules have in this. Observing micronuclei following mitosis can act as a proxy for aneuploidy and aberrant spindle dynamics. It is expected that p53-restored cells would have an increased number of micronuclei, due to their more stable microtubules. And lastly, with the standardization of plusTipTracker, rapid and accurate analysis of a variety of conditions' effects, such as hypoxia, on microtubules can be done to a high degree of ease and certainty, and will remain a powerful tool for years to come.

Methods

Cell culture and plasmid transfections

HeLa cells were grown in DMEM (Sigma-Aldrich, St. Louis, MO) supplemented with 10% fetal bovine serum (FBS; Invitrogen, Carlsbad, CA) and 1X antibiotic/antimycotic (Sigma-Aldrich). For RNA interference (RNAi), transfections were performed 48 hours prior to imaging. For plasmid expression, cells were transfected at least 24 hours prior to imaging using X-tremeGENE HP DNA Transfection Reagent (version 1.0; Roche Diagnostics, Indianapolis, IN) according to the manufacturer's protocol.

RNAi and transient transfection

Cells were grown in 35-mm dishes or MatTek dishes and transfected with siRNAs using GeneSilencer (Genlantis, San Diego, CA) 1 day after plating. siRNA oligonucleotides (Thermo Scientific/Dharmacon, Pittsburgh, PA) used were SMTN1 (Op18-443), 5'-CGUUUGCGAGAGAAGGAUAdtdt-3'p27, and HPV E6 (18E6-385), 5'-CUAACACUGGGUUAUACAAdtdt-3' (restores p53 by depleting the HPV E6 protein; (Goodwin, 2000) SiGenome nontargeting siRNA (Thermo Scientific/Dharmacon) were used as control siRNA sequences for these experiments (Carney and Cassimeris, 2010; Silva 2013).

Western blotting

Soluble cell extracts were prepared as described previously (Carney, 2010), and protein concentrations were measured by Bradford assay. Lysates were diluted in PAGE sample buffer; 20 µg total protein per lane was typically loaded and resolved in 10% polyacrylamide gels and transferred to Immobilon membranes (Millipore, Billerica, MA). Membranes were blocked with 5% nonfat milk in Tris-buffered saline with 0.1% Tween and then probed with primary antibodies: anti-p27 1:1000, anti-p53 1:1000 or anti-stathmin (1:2000; Sigma-Aldrich) followed by secondary antibodies, anti-mouse (1:2000; Abcam, Cambridge, MA) or anti-rabbit (1:10,000; BD Biosciences, Franklin Lakes, NJ) horseradish peroxidase-linked immunoglobulin G. Immunoreactive bands were developed using enhanced chemiluminescence (GE Amersham). Membranes were reprobed with anti- α -tubulin (1:1000; Sigma-Aldrich) or actin (1:1000; Abcam) as a loading control.

Taxol Treatments

Cells were treated with DMSO as a vehicle control in DMEM or Taxol diluted down to 10 nM in DMEM where marked. Taxol was allowed to incubate for 3-4 hours to allow it to come to equilibrium in cells without allowing enough time for widespread cell death.

Imaging and Software

Cells were imaged at 90X at 37° C for 1-5 minutes, contingent of quality of the cell images at a rate of 1 frame every 2 seconds on a Nikon LiveScan Swept Field Confocal Microscope and Nikon NIS-Elements, the corresponding software. The plusTipTracker software was obtained from the Danuser Lab portal at <http://lccb.hms.harvard.edu> and run with MatLab R2008a. For details about how the plusTipTracker software works, see “plusTipTracker: quantitative image analysis software for the measurement of microtubule dynamics”, Applegate 2011. Comets were visualized by transfection with an EB1-GFP plasmid. Cells chosen for imaging displayed low background fluorescence but had prominent comets.

Confocal Microscopy and Immunofluorescence

Cells were fixed, stained, and imaged as described previously (Carney and Cassimeris, 2010). The primary antibody used was mouse anti- α -tubulin; (1:1000; Clone 6-11B-1); rabbit anti-mouse Alexa Fluor 563 (1:200; Gibco-Invitrogen) were used as the secondary antibodies in these experiments. Confocal microscopy was used to image stained cells as described previously (Carney and Cassimeris, 2010).

Statistics

An unpaired Student's T test was used to determine significance.

References:

- Mitchison, Tim, and Marc Kirschner. "Dynamic instability of microtubule growth." *nature* 312.5991 (1984): 237-242.
- Mimori-Kiyosue, Yuko, and Shoichiro Tsukita. "'Search-and-capture' of microtubules through plus-end-binding proteins (+ TIPs)." *Journal of biochemistry* 134.3 (2003): 321-326.
- Risinger, April L., Francis J. Giles, and Susan L. Mooberry. "Microtubule dynamics as a target in oncology." *Cancer treatment reviews* 35.3 (2009): 255-261.
- Goodson, Holly V., Jill S. Dzurisin, and Patricia Wadsworth. "Methods for expressing and analyzing GFP-tubulin and GFP-microtubule-associated proteins." *Cold Spring Harbor Protocols* 2010.9 (2010): pdb-top85.
- Tirnauer, Jennifer S., et al. "EB1-microtubule interactions in *Xenopus* egg extracts: role of EB1 in microtubule stabilization and mechanisms of targeting to microtubules." *Molecular biology of the cell* 13.10 (2002): 3614-3626.
- Piehl, Michelle, et al. "Centrosome maturation: measurement of microtubule nucleation throughout the cell cycle by using GFP-tagged EB1." *Proceedings of the National Academy of Sciences of the United States of America* 101.6 (2004): 1584-1588.
- Matov, Alexandre, et al. "Analysis of microtubule dynamic instability using a plus-end growth marker." *Nature methods* 7.9 (2010): 761-768.
- Applegate, Kathryn T., et al. "plusTipTracker: quantitative image analysis software for the measurement of microtubule dynamics." *Journal of structural biology* 176.2 (2011): 168-184.
- Applegate KT, Danuser G. Technical Report: Using the plusTipTracker Software to Measure and Analyze Microtubule Dynamics from +TIP Comets. 2010
- Belmont, Lisa D., and Timothy J. Mitchison. "Identification of a protein that interacts with tubulin dimers and increases the catastrophe rate of microtubules." *Cell* 84.4 (1996): 623-631.
- Howell, Bonnie, Heather Deacon, and Lynne Cassimeris. "Decreasing oncoprotein 18/stathmin levels reduces microtubule catastrophes and increases microtubule polymer in vivo." *Journal of cell science* 112.21 (1999): 3713-3722.

- Howell, Bonnie, et al. "Dissociation of the tubulin-sequestering and microtubule catastrophe-promoting activities of oncoprotein 18/stathmin." *Molecular biology of the cell* 10.1 (1999): 105-118.
- Sellin, Mikael E., et al. "Global regulation of the interphase microtubule system by abundantly expressed Op18/stathmin." *Molecular biology of the cell* 19.7 (2008): 2897-2906.
- Ringhoff, Danielle N., and Lynne Cassimeris. "Stathmin regulates centrosomal nucleation of microtubules and tubulin dimer/polymer partitioning." *Molecular biology of the cell* 20.15 (2009): 3451-3458.
- Silva, Victoria C., and Lynne Cassimeris. "Stathmin and microtubules regulate mitotic entry in HeLa cells by controlling activation of both Aurora kinase A and Plk1." *Molecular biology of the cell* 24.24 (2013): 3819-3831.
- Brattsand, G. "Correlation of oncoprotein 18/stathmin expression in human breast cancer with established prognostic factors." *British journal of cancer* 83.3 (2000): 311.
- Steinmetz, Michel O. "Structure and thermodynamics of the tubulin–stathmin interaction." *Journal of structural biology* 158.2 (2007): 137-147.
- Gupta, Kamlesh K., et al. "Mechanism for the catastrophe-promoting activity of the microtubule destabilizer Op18/stathmin." *Proceedings of the National Academy of Sciences* 110.51 (2013): 20449-20454.
- Boehm, Manfred, et al. "A growth factor- dependent nuclear kinase phosphorylates p27Kip1 and regulates cell cycle progression." *The EMBO journal* 21.13 (2002): 3390-3401.
- Nguyen, Laurent, et al. "p27kip1 independently promotes neuronal differentiation and migration in the cerebral cortex." *Genes & development* 20.11 (2006): 1511-1524.
- Baldassarre, Gustavo, et al. "p27^{Kip1}-stathmin interaction influences sarcoma cell migration and invasion." *Cancer cell* 7.1 (2005): 51-63.
- Belletti, Barbara, et al. "p27kip1 controls cell morphology and motility by regulating microtubule-dependent lipid raft recycling." *Molecular and cellular biology* 30.9 (2010): 2229-2240.
- Baroni, Timothy E., et al. "A global suppressor motif for p53 cancer mutants." *Proceedings of the National Academy of Sciences of the United States of America* 101.14 (2004): 4930-4935.

- Moll, Ute M., and Alex Zaika. "Nuclear and mitochondrial apoptotic pathways of p53." *FEBS letters* 493.2 (2001): 65-69.
- Murphy, Maureen, Adrian Hinman, and Arnold J. Levine. "Wild-type p53 negatively regulates the expression of a microtubule-associated protein." *Genes & development* 10.23 (1996): 2971-2980.
- Galmarini, C. M., et al. "Drug resistance associated with loss of p53 involves extensive alterations in microtubule composition and dynamics." *British journal of cancer* 88.11 (2003): 1793-1799.
- Giannakakou, Paraskevi, et al. "Enhanced microtubule-dependent trafficking and p53 nuclear accumulation by suppression of microtubule dynamics." *Proceedings of the National Academy of Sciences* 99.16 (2002): 10855-10860.
- Zhang, Christine C., et al. "The role of MAP4 expression in the sensitivity to paclitaxel and resistance to vinca alkaloids in p53 mutant cells." *Oncogene* 16.12 (1998).
- Bacus, Sarah S., et al. "Taxol-induced apoptosis depends on MAP kinase pathways (ERK and p38) and is independent of p53." *Oncogene* 20.2 (2001).
- Wahl, Alan F., et al. "Loss of normal p53 function confers sensitization to Taxol by increasing G2/M arrest and apoptosis." *Nature medicine* 2.1 (1996): 72-79.
- Tan, Guolin, et al. "Apoptosis induced by low dose paclitaxel is associated with p53 upregulation in nasopharyngeal carcinoma cells." *International journal of cancer* 97.2 (2002): 168-172.
- Milas, Luka, et al. "Kinetics of mitotic arrest and apoptosis in murine mammary and ovarian tumors treated with taxol." *Cancer chemotherapy and pharmacology* 35.4 (1995): 297-303.
- Yeung, Tai K., et al. "The mode of action of taxol: apoptosis at low concentration and necrosis at high concentration." *Biochemical and biophysical research communications* 263.2 (1999): 398-404.
- Jordan, Mary Ann, et al. "Mitotic block induced in HeLa cells by low concentrations of paclitaxel (Taxol) results in abnormal mitotic exit and apoptotic cell death." *Cancer research* 56.4 (1996): 816-825.
- Odde DJ, Cassimeris L, Buettner HM. "Kinetics of microtubule catastrophe assessed by probabilistic analysis" *Biophys J.* (1995): 69:796–802

- Cassimeris, Lynne. "The oncoprotein 18/stathmin family of microtubule destabilizers." *Current opinion in cell biology* 14.1 (2002): 18-24.
- Carney, Bruce K., and Lynne Cassimeris. "Stathmin/oncoprotein 18, a microtubule regulatory protein, is required for survival of both normal and cancer cell lines lacking the tumor suppressor, p53." *Cancer Biol Ther* 9.9 (2010): 699-709.
- Godin, Juliette D., et al. "p27^{kip1} Is a Microtubule-Associated Protein that Promotes Microtubule Polymerization during Neuron Migration." *Developmental cell* 23.4 (2012): 729-744.
- Ishida, Noriko, et al. "Phosphorylation of p27 Kip1 on serine 10 is required for its binding to CRM1 and nuclear export." *Journal of Biological Chemistry* 277.17 (2002): 14355-14358.
- Steinmetz, Michel O. "Structure and thermodynamics of the tubulin–stathmin interaction." *Journal of structural biology* 158.2 (2007): 137-147.
- Song, Yuhong, Carol Wong, and David D. Chang. "Overexpression of wild-type RhoA produces growth arrest by disrupting actin cytoskeleton and microtubules." *Journal of cellular biochemistry* 80.2 (2001): 229-240.
- Besson, Arnaud, Richard K. Assoian, and James M. Roberts. "Regulation of the cytoskeleton: an oncogenic function for CDK inhibitors?." *Nature Reviews Cancer* 4.12 (2004): 948-955.
- Hoppe-Seyler, F., and K. Butz. "Repression of endogenous p53 transactivation function in HeLa cervical carcinoma cells by human papillomavirus type 16 E6, human mdm-2, and mutant p53." *Journal of virology* 67.6 (1993): 3111-3117.
- Goodwin, Edward C., and Daniel DiMaio. "Repression of human papillomavirus oncogenes in HeLa cervical carcinoma cells causes the orderly reactivation of dormant tumor suppressor pathways." *Proceedings of the National Academy of Sciences* 97.23 (2000): 12513-12518.

Cody Molnar

CONTACT INFORMATION

Permanent Address: 276 Delfire Road, Elton, PA 15934
Phone: 814-270-6266
Email: cam812@lehigh.edu

EDUCATION

Bachelor of Science, Molecular Biology

Lehigh University, Bethlehem PA
GPA: 3.44
Honors Thesis: Crisp2 Relocalization During Sperm Capacitation
Graduation Date: 05/12

Master of Science, Molecular Biology

Lehigh University, Bethlehem PA
GPA: 3.74
Masters Thesis: Applying Automated Tracking of Microtubules using plusTipTracker
Expected Graduation Date: 05/14

RESEARCH EXPERIENCE

- | | |
|---|------------------|
| SEA Lab | 08/10-12/10 |
| Lehigh University, Bethlehem PA | |
| <ul style="list-style-type: none">• Isolated and purified novel bacteriophages of E. Coli from local environments• Purified viral DNA to be sent for sequencing• Identified and cataloged viral genome for future studies• Worked in a group setting | |
| Undergraduate Honors Research, Andrology Laboratory | 12/10-05/12 |
| Lehigh University, Bethlehem PA | |
| <ul style="list-style-type: none">• Collected and processed human semen samples using NIH guidelines on human subjects and bio-hazardous material• Performed metabolic assays to assess possible activities of a novel enzyme, α-L-Fucosidase• Tested efficacy of novel spermicides and surfactants for possible FDA approval• Identified CRISP2 translocation and proposed a mechanism of action in human sperm | |
| Master's Thesis Research, Microtubule Laboratory | 9/12- To Present |
| Lehigh University, Bethlehem PA | |
| <ul style="list-style-type: none">• Mastered use of a large variety of microscopy techniques, including Live-Cell, Confocal, and basic fluorescence microscopy• Researched and adapted automated tracking software responsible for data analysis• Used multiple techniques to assess cell cycle regulation in cancerous cell lines• Synthesized information from multiple experiments to form a cohesive understanding of protein | |

interactions with microtubules

- Mastered many core techniques in molecular biology, including, but not limited to, cell culture, transfections, cell cycle synchronization and western blotting
- Responsible for general lab upkeep

PUBLICATIONS

Robert V. Skibbens, Jennifer M. Colquhoun, Megan J. Green, Cody A. Molnar, Danielle N. Sin, Brian J. Sullivan, Eden E. Tanzosh 'Cohesinopathies of a feather flock together' PLoS genetics 9.12 (2013): e1004036.

L. Cassimeris, V. Caruso Silva, E. Miller, Q. Ton, C. Molnar, and J. Fong. 'Fueled by Microtubules: Does tubulin dimer/polymer partitioning regulate intracellular metabolism?' Cytoskeleton 2012, 69:133-143